Acoustic emission and digital image correlation evidence of size effects on the compression failure of concrete

Acoustic Emission and Digital Image Correlation Evidences of Size Effects on the Compression Failure of Concrete

Zihan Jiang [1], Zhiwen Zhu [2], Federico Accornero [3], Giuseppe Lacidogna [4]

[1] Ph.D. Student, Department of Civil Engineering and Smart Cities, Shantou University, Shantou, China. ORCID: https://orcid.org/0009-0002-5327-2512. Email: 19zhjiang@stu.edu.cn.

[2] Professor, Department of Civil Engineering and Smart Cities, Shantou University, Shantou, China. ORCID: https://orcid.org/0000-0003-3309-179X. Email: zhuzw@stu.edu.cn. (corresponding author: zhuzw@stu.edu.cn)

[3] Associate Professor, Department of Civil Engineering and Smart Cities, Shantou University, Shantou, China. ORCID: https://orcid.org/0000-0002-9638-8411. Email: federico@stu.edu.cn

[4] Professor, Department of Structural, Geotechnical and Building Engineering, Politecnico di Torino, Turin, Italy. ORCID: https://orcid.org/0000-0002-0192-3793. Email: giuseppe.lacidogna@polito.it.

*Corresponding author: giuseppe.lacidogna@polito.it (G. Lacidogna); zhuzw@stu.edu.cn (Z. Zhu);

Abstract: Compression failure of concrete without effective confinement may show brittle failure modes, size effects being crucial for understanding catastrophic behaviours. Compression tests are performed to investigate the emitted energy during snap-back instabilities of concrete specimens having different sizes and slenderness ratios. Plain concrete specimens with sizes equal to 75, 150, and 300 mm, and slenderness ratios equal to 0.5, 1.0, and 2.0, are monitored using acoustic emission (AE) and digital image correlation (DIC) techniques. The results show the compression strength and ductility exhibit strong size and slenderness effects. As size or slenderness scale becomes larger, the failure behaviour exhibits a ductile-to-brittle transition, with the post-peak branch shifting from softening to catastrophic, showing local and global instability phenomena. In

particular, as the specimen slenderness increases, the final collapse shows a crushing-to-cracking failure transition, as also evidenced by the DIC technique. In brittle cases, crack propagation suddenly occurs with a catastrophic drop in load-carrying capacity, and the resulting emitted energy appears with a burst in cumulated AE curves, confirming that AE energy arises from snap-back instabilities in the structural response. This research has significant implications for the structural reliability and safety concrete structures, reducing the risk of catastrophic failure.

Keywords: Acoustic Emission; Digital Image Correlation; Concrete; Compression; Size effects; Ductile-to-brittle transition

1. Introduction

Compressive failure of brittle materials such as concrete is mainly characterised by microcrack nucleation, growth, and coalescence, over wide ranges of time and size scales (Carpinteri *et al*., 2013). According to experimental evidence, the post-peak phase of the loading process is characterized by a strong strain localization. In the softening regime, energy dissipation occurs over a damaged surface rather than within the entire specimen volume (Carpinteri *et al*., 2007).

Previous research has confirmed that concrete, as a quasi-brittle material, exhibits a significant size effect on its material properties according to the change in the characteristic structural size. Specifically, small specimens demonstrate higher strength than large ones, the structural material being unchanged. Over recent decades, several size effect laws for concrete have been proposed, including Weibull's statistical theory (Weibull, 1951), boundary effect model (Duan *et al*., 2002), Bazant's size effect law (Bazant *et al*., 2007), and Carpinteri's multifractal

scaling law (MFSL) (Carpinteri *et al*., 1995). Carpinteri's MFSL is based on the fractal theory, describing the damage of quasi-brittle materials in a non-integer dimensional space. Additionally, numerical simulations become a supplementary method for exploring the size effect of cementitious materials (Jin *et al*., 2019; Zhang *et al*., 2018). Various approaches, such as the cohesive model (Feng *et al*., 2018), nonlocal continuum damage model (Marzec *et al*., 2019) and discrete element method (Sinaie, 2017), have been used to simulate the size effect of cementitious materials (Muciaccia *et al*., 2017; Chen *et al*., 2018).

Based on fracture mechanics, Li *et al*. (2018) investigated the effect of shapes and sizes on compressive strength using cube and cylindrical concrete specimens of varying sizes, whereas Fladr *et al*. (2017) examined the correlation between specimen size and compressive strength of high-strength fibre-reinforced concrete. In addition, Balla *et al*. (2023) investigated the effect of specimen sizes on the compressive performance of hybrid FRP-strengthened RC square columns. Jin *et al*. (2020) assessed the compression behaviour of geometrically similar RC columns with varying specimen sizes, demonstrating that the compressive strength exhibited a significant size effect. Recently, advanced monitoring techniques, such as acoustic emission (AE) (Alam *et al*., 2015), and digital image correlation (DIC) (Keerthana *et al*., 2020), have provided new insights into the effect of specimen sizes on the energy release rate, crack initiation, and the fracture process zone.

It is reported that the load-displacement curve changes significantly by varying the size scale, the structural shape remaining unchanged (Carpinteri *et al*., 1989). The softening branch in the load-displacement curve becomes steeper when the size increases. For size scales larger than the critical one, the post-peak branch presents a positive slope. In more brittle cases, crack propagation occurs suddenly with a catastrophic drop in the load-carrying capacity. This means that both load

and displacement must decrease in order to have a controlled crack propagation (Carpinteri *et al*., 2018). Such a phenomenon, the so-called snap-back instability (see Fig.1), was deeply investigated concerning crack growth analysis in elastic-softening materials.

The size-scale transition from ductile to brittle behaviour is governed by a non-dimensional brittleness number, S_E, which is a function of material properties and structure size. A truly brittle failure occurs only with relatively low fracture energies G_{IC}, high tensile strengths σ_u, or large structure size-scales b, i.e. when $S_E = G_{IC}/\sigma_u b \rightarrow 0$. On the other hand, if the loading process is controlled by a monotonically increasing displacement over time, the snap-back instability can be experimentally captured (Carpinteri *et al*., 2019).

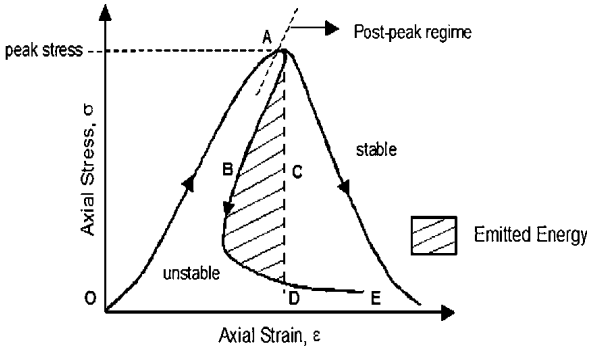

Fig.1. Stable and catastrophic (snap-back) response (modified from Lacidogna *et al*., 2019)

Currently, many studies on size effects in quasi-brittle materials can be found in the scientific literature. However, concrete materials are used in a wide range of engineering applications, especially for large structures, and their size effects need to be investigated in terms of size-slenderness effect. In particular, AE techniques can provide new insights in concrete size effect on the energy release rate by means of the fractal theory, which describes the concrete damage in a non-integer dimensional space.

From an engineering perspective, understanding the size and slenderness effects on concrete's compressive behavior is highly relevant for large-scale structural applications. In real-world engineering projects, such as dams, high-rise buildings, and bridges, where concrete elements are subjected to significant compressive forces, size effects directly impact the performance and safety of these structures. By addressing these effects, this research provides valuable insights for structural engineers to better design concrete components with appropriate dimensions, ensuring enhanced safety and durability against catastrophic failures, particularly in large-scale structures where the traditional assumptions of small-scale testing may not apply.

This paper presents an experimental investigation on concrete damage using integrated AE and DIC techniques. Plain concrete specimens with different volumes are tested to investigate the size-slenderness effect. The DIC method gives a precise full-field strain measurement, while AE signals resulting from internal damage are analysed. The emitted energy is experimentally detected during snap-back instabilities of concrete specimens in compression. In more brittle cases, crack propagation suddenly occurs with a catastrophic drop in the load-carrying capacity, so the resulting emitted energy appears with a burst in cumulated AE curves. In particular, the size-slenderness effect is employed to evaluate damage domain and fractal dimension.

2. Emitted energy and snap-back instability

Some information on the modalities of energy release and the development of cracking patterns can be obtained on the basis of the AE monitoring technique (Aggelis *et al*., 2011, 2013; Lacidogna *et al*., 2020; Jiang *et al*., 2024a). AE technique provides a non-destructive monitoring method to detect the damage evolution in materials and structures (Zhu *et al*., 2024; Jiang *et al*., 2024b; Li *et al*., 2020). AE waves can be measured by sensors placed on the structural element

surface, providing crucial information on crack initiation and propagation (Zheng *et al*., 2022; Wang *et al*., 2024; Han *et al*., 2019).

Recently, it has been shown that the energy emission is proportional to the total number of AE signals, and it is a surface-prevailing phenomenon. This has been demonstrated by interpreting AE data with statistical and fractal concepts (Carpinteri *et al*., 2007). Furthermore, according to the recent interpretations (Carpinteri *et al*., 2018), the relationship between crack propagation and emitted energy, if analysed by AE, is represented by the area subtended by each snap-back branch (see Fig.2). The total energy released during the test, R, is equal to the dissipated energy, D, plus the emitted energy during the snap-back phenomena, E.

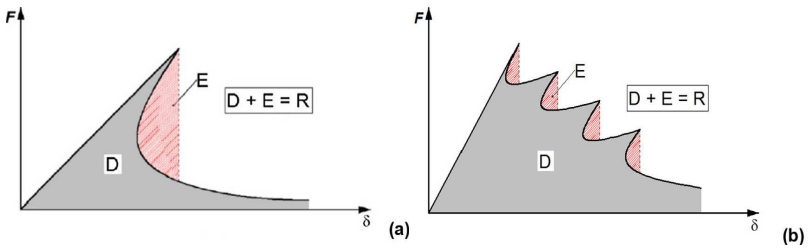

Fig.2. Load-displacement curves representing: (a) a catastrophic behaviour (single snap-back); (b) a global softening behaviour perturbed by multiple local instabilities (snap-back) (modified from Carpinteri *et al*., 2018).

The mechanical behaviour of compressive specimens can be described in three stages (Carpinteri *et al*., 2009). The first stage involves the initiation and propagation of microcracks. Approaching the compressive strength, such microcracks coalesce to form macrocracks, localizing over a preferential surface. In the second stage, the ultimate compressive strength, σ_u, is reached, and the inelastic deformations are localized in a crushing band. In the final stage, the material in the crushing zone is damaged. By varying the geometrical parameters of specimens, different global responses in the stress-strain diagram can be obtained (Lacidogna *et al*., 2013).

In particular, the softening process under displacement control is stable when the slope in the softening regime is negative (Fig.1), and a sudden drop in the load-bearing capacity occurs when the slope is infinite. The overall behaviour of specimens in compression depends on geometrical (size and slenderness) and mechanical (crushing energy and compression strength) parameters (Carpinteri *et al*., 2013). Following previous studies (Carpinteri *et al*., 2009), a catastrophic softening (snap-back) occurs when the global brittleness, B, is:

$$B = \frac{S_{E,c}}{\varepsilon_c \lambda} \leq \frac{1}{2.3} \tag{1}$$

where $\lambda = l/b$ is the specimen slenderness ratio, and b is the specimen base size. ε_c is the critical compression strain, and $S_{E,c}$ is the energy brittleness number in compression. Therefore, the stability of the compression process is governed by Eq.(1).

In this investigation, an experimental correlation is verified between the emitted energy (E) and global or local snap-back instabilities of concrete block specimens in compression.

3. Testing plain concrete block specimens

3.1 Block specimens

Brittle materials usually contain pre-existing microcracks, which can control the failure mechanism and affect the structural strength (Marolt *et al*., 2018; Morgan *et al*., 2013). In this framework, the AE technique has been effectively applied in the analysis of fracture phenomena and fault growth (Chang *et al*., 2004).

As listed in Table 1, the plain concrete used in this study is made using ordinary Portland

155 cement type 42.5, grade II fly ash, grade S95 slag powder, crushed gravel with diameter 5-25 mm,
156 and mechanical sand with a fineness modulus of 3.1. The composition ratio of
157 cement:sand:stone:water is 1:2.24:2.97:0.48. The compressive strength of concrete is equal to 33.2
158 MPa after curing for 28 days.

159

160 Table 1 Concrete strength and mix ratio

Concrete grade	f_{cu} (MPa)	Water-binder ratio	Sand rate (%)	Fly ash (wt/%)	Slag powder (wt/%)	Material usage (kg/m^3)					
						Cement	Fly ash	Slag powder	Sand	Stone	Water
C25	33.2	0.48	43	28	14	201	100	50	785	1044	170

161

162 In this section, the results of compression tests carried out on nine specimens (3×3) having
163 size of 75, 150, and 300 mm, and slenderness 0.5, 1.0, and 2.0, are presented (see Table 2 and
164 Fig.3). The test phases are illustrated Fig.4.

165

166 Table 2. Specimen sizes (unit: mm)

Series	Dimension (mm)	Slenderness ratio
I	75 × 75 × 37	0.5
	75 × 75 × 75	1.0
	75 × 75 × 150	2.0
II	150 × 150 × 75	0.5
	150 × 150 × 150	1.0
	150 × 150 × 300	2.0
III	300 × 300 × 150	0.5
	300 × 300 × 300	1.0
	300 × 300 × 600	2.0

167

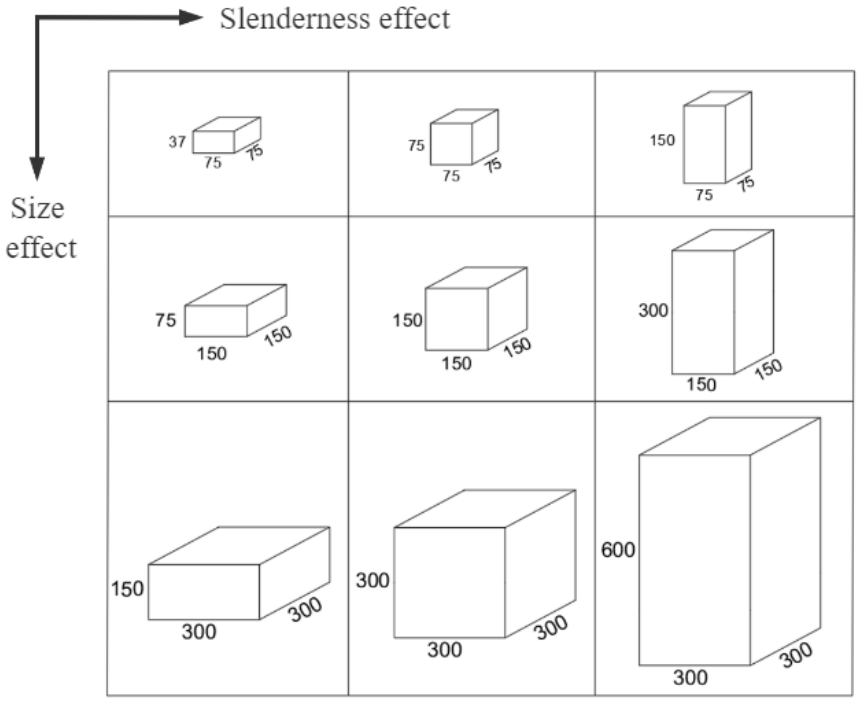

Fig.3. Size-slenderness variation

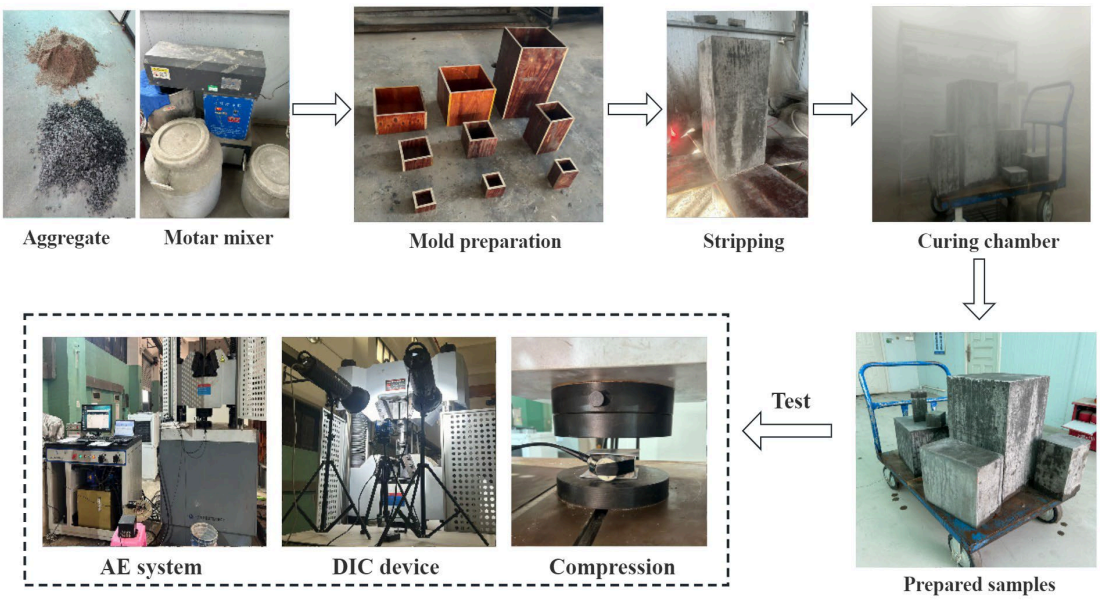

Fig.4. Test phases

3.2 AE monitoring setup

During the experimental tests, the specimens are equipped with a thin layer of Teflon (Fig.5) in contact between the platen of the testing machine and the specimen ends, to significantly reduce the friction force and facilitate the transversal deformation. The loading process adopts a displacement-control with a constant rate equal to 0.01 mm/s.

Each specimen is monitored by means of the AE technique. The AE system utilized in this test is the ÆMISSION®, equipped with piezoelectric sensors in the range 10kHz-1MHz. Each channel has independent threshold triggers, automatically extracting AE signal parameters for continuous monitoring. The sensor is glued with silicone resin on the specimen surface, as depicted in Fig.5. The AE waves captured by the sensors were amplified with 60 dB gain before being processed, setting the acquisition threshold level up to 2 mV. In all experiments, the loading is stopped when dropping to the 20% of the peak load.

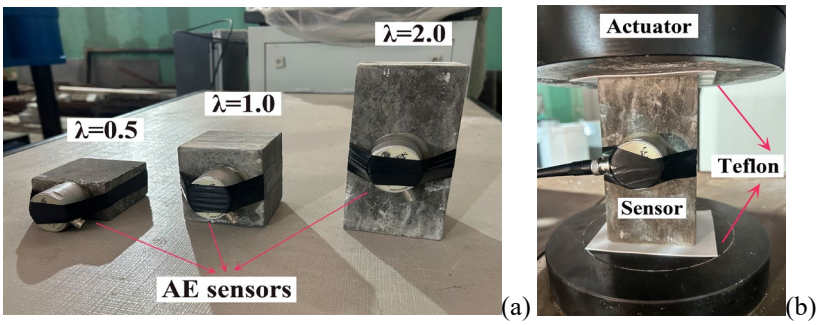

Fig.5. AE sensor layout (a) and compression tests (b)

4. Experimental results

4.1 Slenderness effect

The loading history and the final collapse for three specimens with size 150 mm and

193 slenderness 0.5, 1.0, and 2.0 are shown in Fig.6 and Fig.7. As expected, the more slender specimen
194 ($\lambda = 2.0$) exhibited a brittle behaviour with global snap-back instability, the post-peak branch being
195 almost vertical compared to that of the stubby specimens ($\lambda = 0.5$), which is characterized by a
196 softening post-peak response.

197 As regards the concrete specimen with slenderness $\lambda = 2.0$ (Fig.6d), two severe global snap-
198 back instabilities were detected in the post-peak branch of the loading response (see Fig.7c). A
199 correlation emerges between the catastrophic drops (snap-back instabilities) and the AE bursts
200 (emitted energy, E) in the cumulated AE curve. The failure mode observed during the experiment
201 is governed by a dominant sub-vertical crack (Fig.6d).

202 The result of the concrete specimen with slenderness $\lambda = 1.0$ is shown in Fig.7b. Its behaviour
203 is characterized by a global snap-back instability just after the peak load. At the same time, an AE
204 burst (emitted energy, E) is detected in the cumulated curve.

205 The loading behaviour of the specimen with slenderness $\lambda = 0.5$ is shown in Fig.7a. It is
206 characterized by a ductile response in the post-peak stage. The softening post-peak regime is
207 perturbed by the loading drops (local snap-back instabilities), generating AE jumps (emitted
208 energy, E) in the cumulated curve. The final collapse exhibits significant crushing characteristics
209 (Fig.6b).

210 In general, as the specimen changes from stubby to slender (λ varying from 0.5 to 2), the final
211 collapse shows a crushing-to-cracking failure transition, together with a transition from local-to-
212 global snap-back instabilities, and a decrease in the compressive strength (Fig.7).

213

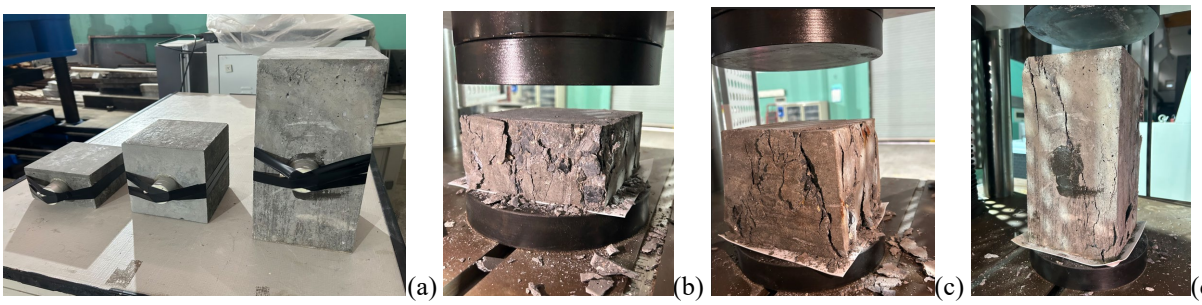

Fig.6. Final collapse for concrete specimens (a) with size of 150 mm, and slenderness (b) λ = 0.5, (c) λ = 1.0, and (d) λ = 2.0.

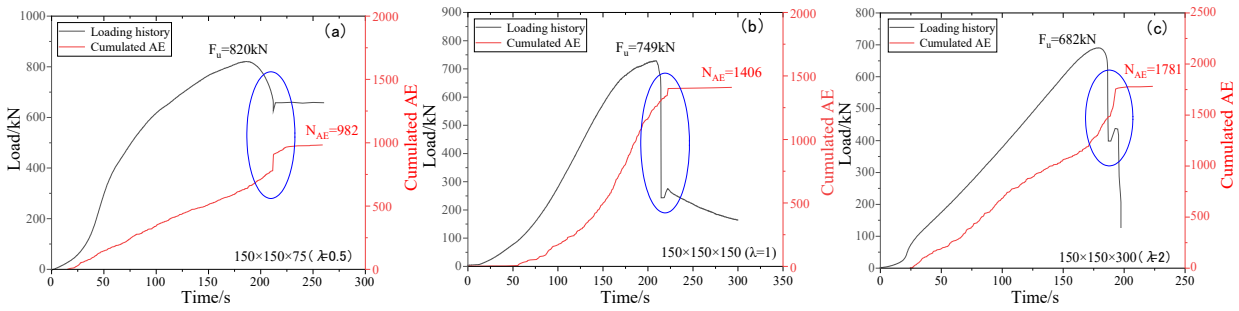

Fig.7. Loading history and cumulated AE curve for concrete specimens with slenderness equal to (a) λ = 0.5, (b) λ = 1, and (c) λ = 2.0, and size of 150 mm. A correlation emerges between loading drops (snap-back instabilities) and AE jumps (emitted energy, E).

4.2 Size effect

The loading behaviour of three specimens with the slenderness equal to 1 (Fig.8), and sizes equal to 75 mm, 150 mm, and 300 mm are shown in Fig.9. The largest specimen (Fig.8c) exhibited a more brittle behaviour with global snap-back instability (Fig.9c), the post-peak branch being almost vertical compared to that of the smallest specimens, which is characterized by a softening response. Moreover, an evident correlation emerges between the catastrophic drops in the post-peak regime of the loading process and the AE bursts in the cumulated curve.

The result of the concrete specimen with size of 150 mm (Fig.8b) is shown in Fig.9b. A global snap-back instability is detected just after the peak load, corresponding to an AE burst in the cumulated curve.

The loading behaviour of the specimen with size of 75 mm (Fig.8a) is shown in Fig.9a, showing a softening response. This post-peak regime is perturbed by small local snap-back instabilities (Fig.9a), generating AE jumps in the cumulated curve.

Generally speaking, as the specimen size increases, the structural behaviour exhibits a ductile-to-brittle transition, and the post-peak response changes from softening to snap-back, with local-to-global snap-back transition (Fig.9).

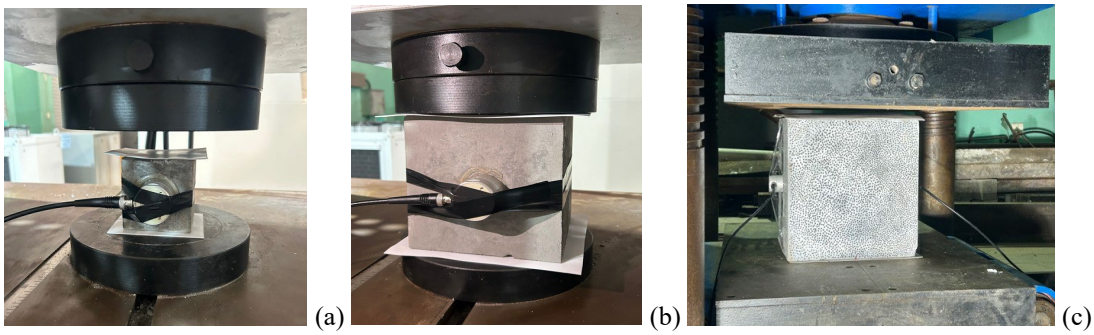
(a) (b) (c)

Fig.8. Loading layouts for specimens with slenderness equal to1 and size of (a) 75 mm, (b) 150 mm, and (c) 300 mm.

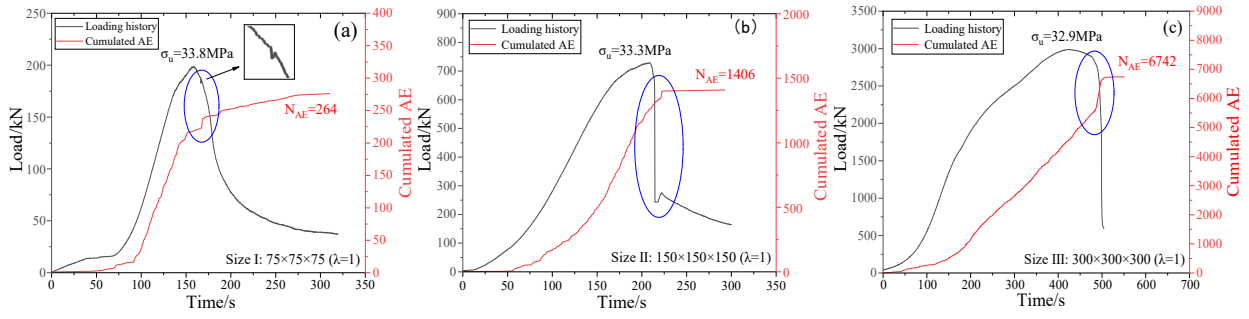

Fig.9. Loading history and cumulated AE curve for concrete specimens with slenderness equal to 1 and size of (a) 75 mm, (b) 150 mm, and (c) 300 mm. A correlation emerges between loading drops (snap-back instabilities) and AE jumps (emitted energy, E).

4.3 DIC monitoring

The DIC technique is a non-contact optical measurement method that tracks the motion of points on a surface by analysing the randomly distributed speckle patterns, facilitating real-time observation of surface displacement and strain (Boniface *et al*., 2019; Zhou *et al*., 2016; Alam *et al*., 2015; Zhang *et al*., 2023).

The final collapse for three specimens with size of 300 mm and slenderness of 0.5, 1.0, 2.0, is shown in Fig.10a-c. Before loading, a matte black paint coat is applied to the specimen surface to generate speckle patterns, with the speckle size ranging between 5 and 7 pixels. During the loading process, the DIC technique is employed for real-time recording, as illustrated in Fig.10d. Subsequently, the image analysis system is used to detect the surface displacement and calculate the full-field strain.

Fig.11 displays the strain cloud diagram depicting the fracture process in concrete specimens with different slenderness, obtained by DIC technique. As shown in Fig.11c, the more slender specimen ($\lambda = 2.0$) exhibits a typical brittle fracture characterized by a dominant near-vertical crack occurring catastrophically (Fig.10c), together with fewer cracks with larger crack widths. Conversely, the stubby specimens ($\lambda = 0.5$) show a ductile fracture characterized by several sub-vertical cracks, with a gradual increase in the number of cracks (Fig.11a). Moreover, the final collapse shows notable crushing failure (Fig.10a).

In summary, as the specimen shifts from stubby to slender, the structural behaviour of the concrete specimens gradually changes from ductile to brittle, with the final collapse moving from crushing to cracking.

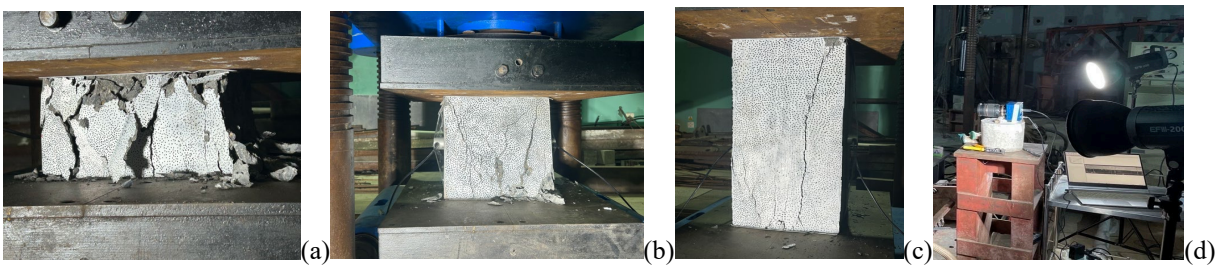

Fig.10. Final collapse for concrete specimens with size of 300 mm and slenderness equal to (a) λ = 0.5, (b) λ = 1.0, and (c) λ = 2.0. DIC monitoring (d).

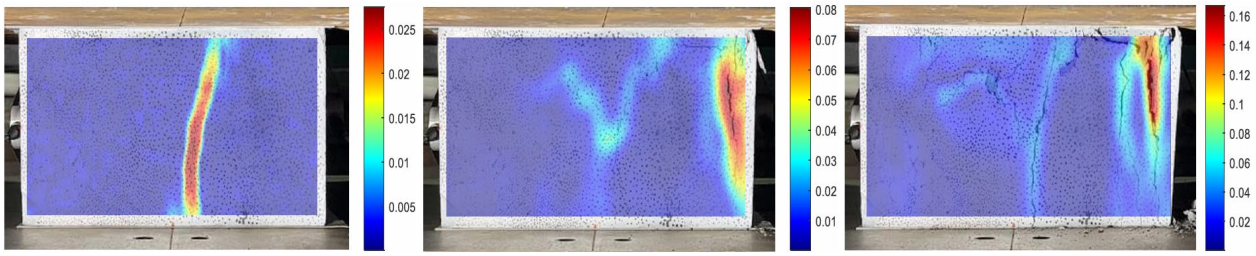

(a) λ=0.5

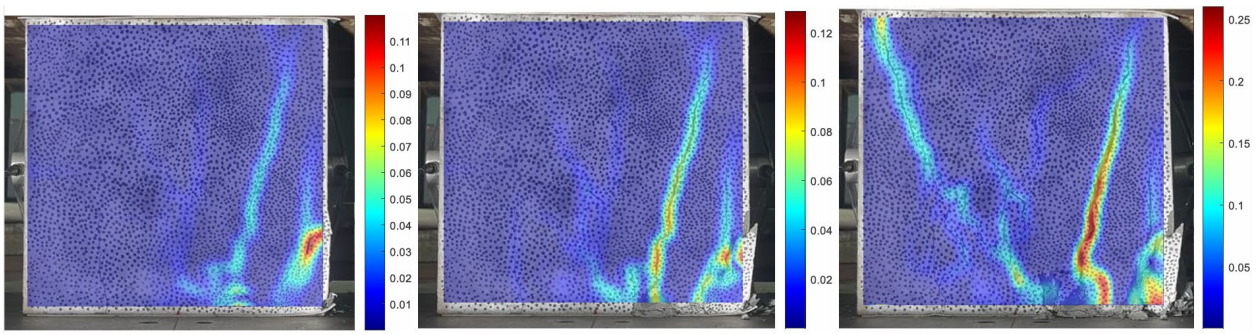

(b) λ=1.0

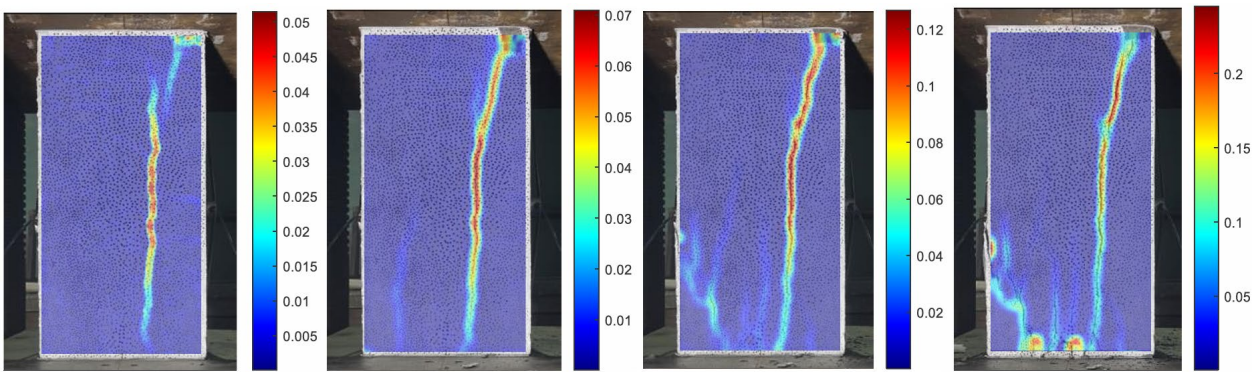

(c) λ=2.0

Fig.11. DIC strain cloud diagram of the fracture process in concrete specimens with size equal to 300 mm and slenderness equal to (a) λ = 0.5, (b) λ = 1.0, and (c) λ = 2.0.

5. Fractal domain of emitted energy

Considering the fragmentation theory, the energy detected during microcrack propagation, E, is emitted over a fractal domain comprised between a surface and a volume (Carpinteri *et al*., 2012). Therefore, the following size-scaling law is assumed for the energy emission during fragmentation:

$$E \propto V^{D/3} \tag{2}$$

where the fractal exponent, D, is comprised between 2.0 and 3.0. Considering L as the characteristic dimension of the specimen, thus, $V^{D/3} = L^{3(D/3)} = L^{D}$. If $D = 3$, the damage will be distributed in the whole specimen volume. On the contrary, if $D = 2$, the damage will be organized on a preferential surface.

This indicates that the fractal energy density (having non-integer physical dimensions),

$$\Gamma = \frac{E}{V^{D/3}}, \tag{3}$$

can be considered as the size-independent parameter (Lacidogna *et al*., 2019).

Furthermore, AE can be detected during microcrack propagation. The energy emission, E, is proportional to the total number $N_{\max}$ of AE signals (Lacidogna *et al*., 2019). Accordingly, the total number of AE signals, $N_{\max}$, over a fractal domain, can be considered as the size-independent parameter:

$$\Gamma_{\mathrm{AE}} = \frac{N_{\max}}{V^{D/3}} \tag{4}$$

where Γ_{AE} is the value of AE signals fractal density.

The total number of AE signals and loading history from nine specimens with different volumes is shown in Fig.12. It has been observed that compressive strength and ductility exhibit a strong size-slenderness effect by changing the specimen volume. The size-slenderness effect on N_{max} is represented as a function of the specimen volume (Fig.13). The log-log diagram shows a slope close to 0.73, i.e. a fractal dimension equal to 2.19, emphasizing that the energy emission occurs in a fractal domain close to a surface. Thus, the fractal AE density is 4 $cm^{-2.19}$, i.e. 4 signals per unit surface.

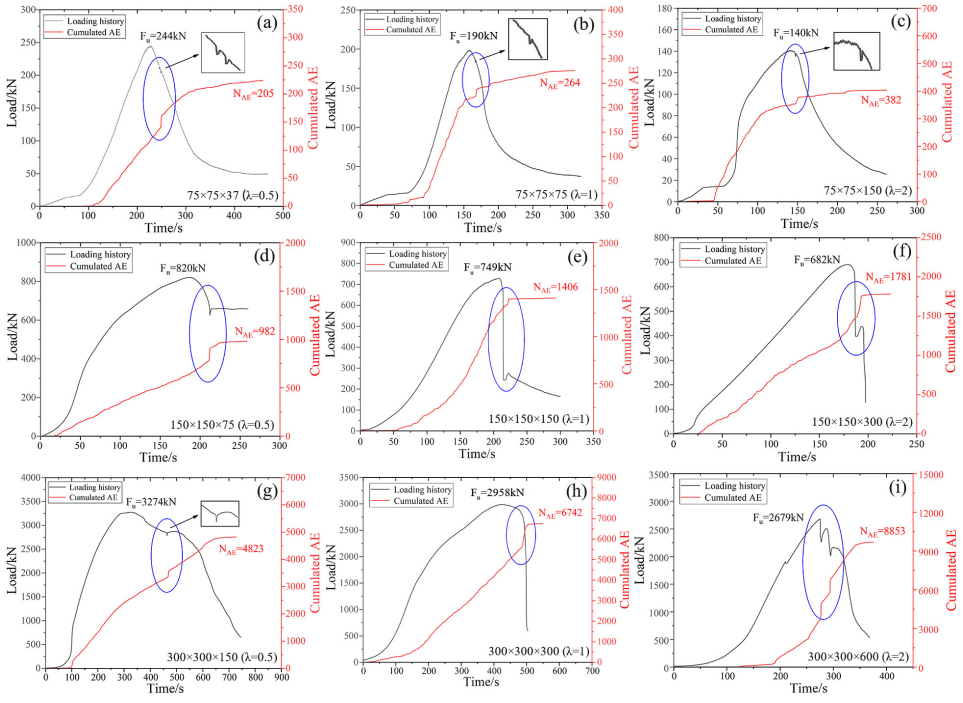

Fig.12. Loading history and cumulated AE curve for different specimen volumes with slenderness equal to 0.5, 1.0, and 2.0, and sizes of 75, 150, and 300 mm.

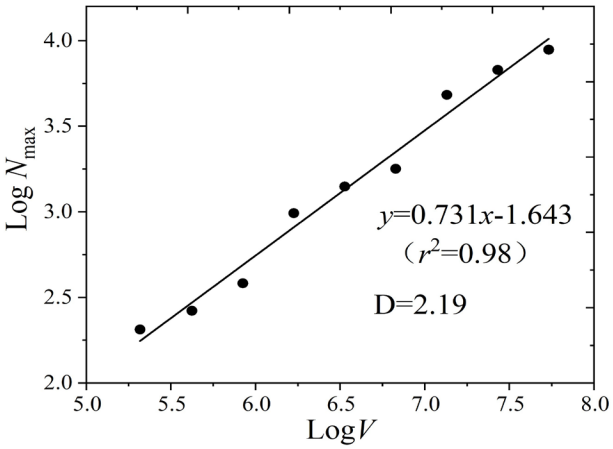

Fig.13. Fractal domain of energy emission.

6. Conclusions

In this paper, the results of experimental tests carried out on plain concrete specimens are analysed, to demonstrate that the emitted energy is generally due to snap-back instabilities. Concrete specimens with different sizes and slenderness ratios are considered, and all the tests are monitored using integrated AE and DIC techniques. The conclusions are as follows.

(1) As the size-slenderness increases, the compressive strength decreases, and the structural behaviour exhibits a ductile-to-brittle transition, with the post-peak response changing from softening to snap-back. In addition, as the specimens change from stubby to slender, the final collapse shows a crushing-to-cracking failure transition, as evidenced by the DIC technique.

(2) For large and slender specimens (size$\geqslant$150mm and $\lambda\geqslant$1), the crack propagation occurs suddenly with a catastrophic drop in the load-carrying capacity, and the resulting emitted energy appears with a burst in the cumulated AE curve. In contrast, for small and stubby specimens (size=75mm or λ=0.5), the softening post-peak regime is perturbed only by local snap-back instabilities.

(3) The fractal domain of the emitted energy presents a dimension equal to 2.19, emphasizing that AE occur in a fractal domain close to a surface. In particular the AE density is equal to 4 signals per unit surface.

The findings provide valuable data on the role of size and slenderness in concrete failure modes, with significant implications for engineering applications in large concrete structures. Understanding size effects and the ductile-to-brittle transition helps optimize the design of concrete components in large infrastructures, preventing catastrophic failures. This study highlights the importance of considering these factors in designing structures like skyscrapers, dams, and bridges. The integration of AE and DIC techniques offers a reliable method to assess and predict concrete failure modes, enhancing safety and serviceability in real-world applications.

Credit authorship contribution statement

Zihan Jiang: Writing – original draft, Methodology, Investigation, Data curation, Conceptualization. **Zhiwen Zhu**: Writing – review & editing, Methodology, Data curation, Conceptualization. **Federico Accornero**: Methodology, Supervision, Conceptualization, Writing-Review & Editing. **Giuseppe Lacidogna**: Writing–review & editing, Project administration, Methodology, Investigation, Funding acquisition, Data curation, Conceptualization.

Declaration of competing interest

The authors declare that they have no known competing financial interests or personal relationships that could have appeared to influence the work reported in this paper.

Data availability statement

Some or all data, models, or code that support the findings of this study are available from the corresponding author upon reasonable request.

Acknowledgements

The authors wish to acknowledge the National Natural Science Foundation of China (52278509), the International Training Program for Outstanding Young Scientific Research Talents of Shantou University, the STU Outstanding Talent Grant N. 140-09423016, and the sponsorship guaranteed with basic research funds provided by Politecnico di Torino, Italy for their financial aids in this work.

References

Aggelis DG (2011) Classification of cracking mode in concrete by acoustic emission parameters. *Mechanics Research Communications* **38**:153–157.

Aggelis DG, Mpalaskas AC and Matikas TE (2013) Investigation of different fracture modes in cement-based materials by acoustic emission. *Cement and Concrete Research* **48**:1-8.

Alam SY, Loukili A, Grondin F and Rozière E (2015) Use of the digital image correlation and acoustic emission technique to study the effect of structural size on cracking of reinforced concrete. *Engineering Fracture Mechanics* **143**:17–31.

Balla TMR, Prakash SS and Rajagopal A (2023) Role of size on the compression behaviour of hybrid FRP strengthened square RC columns–Experimental and finite element studies. *Composite Structures* **303**:116314.

383 Bazant ZP, Vorechovsky M and Novak D (2007) Asymptotic prediction of energetic statistical size effect
384 from deterministic finite-element solutions. *Journal of Engineering Mechanics* **133(2)**:153–162.
385 Boniface A, Saliba J, Sbartaï Z M, Ranaivomanana N and Balayssac JP (2020) Evaluation of the acoustic
386 emission 3D localisation accuracy for the mechanical damage monitoring in concrete. *Engineering*
387 *Fracture Mechanics* **223**:106742.
388 Carpinteri A (1989) Size effects on strength, toughness, and ductility. *Journal of Engineering Mechanics*
389 **115**:1375–1392.
390 Carpinteri A, Chiaia B and Ferro G (1995) Structures, size effects on nominal tensile strength of concrete
391 structures: multifractality of material ligaments and dimensional transition from order to disorder.
392 *Materials and Structures* **28(6)**:311–317.
393 Carpinteri A, Lacidogna G and Pugno N (2007) Structural damage diagnosis and life-time assessment by
394 acoustic emission monitoring. *Engineering Fracture Mechanics* **74**:273–289.
395 Carpinteri A, Corrado M, Paggi M and Mancini G (2009) The overlapping crack model for uniaxial and
396 eccentric concrete compression tests. *Magazine of Concrete Research* **61**:745–757.
397 Carpinteri A, Corrado M and Lacidogna G (2012) Three different approaches for damage domain
398 characterization in disordered materials: fractal energy density, b-value statistics, renormalization group
399 theory. *Mechanics of Materials* **53**:15–28.
400 Carpinteri A, Corrado M and Lacidogna G (2013) Heterogeneous materials in compression: correlations
401 between absorbed, released and acoustic emission energies. *Engineering Failure Analysis* **33**:236–250.
402 Carpinteri A and Accornero F (2018) Multiple snap-back instabilities in progressive microcracking
403 coalescence. *Engineering Fracture Mechanics* **187**:272–281.
404 Chang SH and Lee CI (2004) Estimation of cracking and damage mechanisms in rock under triaxial
405 compression by moment tensor analysis of acoustic emission. *International Journal of Rock Mechanics*
406 *and Mining Sciences* **41**(7):1069–1086.
407 Chen P, Liu CY and Wang YY (2018) Size effect on peak axial strain and stress-strain behaviour of concrete

subjected to axial compression. *Construction and Building Materials* **188**: 645–55.

Duan K, Hu X and Wittmann F (2002) Explanation of size effect in concrete fracture using non-uniform energy distribution. *Materials and Structures* **35(6)**:326–331.

Feng DC and Wu JY (2018) Phase-field regularized cohesive zone model (CZM) and size effect of concrete. *Engineering Fracture Mechanics* **197**:66–79.

Fladr J and Bílý P (2017) Specimen size effect on compressive and flexural strength of high strength fibre-reinforced concrete containing coarse aggregate. *Composites Part B-Engineering* **138**: 77–86.

Han QH, Yang G, Xu J, Fu ZW, Lacidogna G and Carpinteri A (2019) Acoustic emission data analyses based on crumb rubber concrete beam bending tests. *Engineering Fracture Mechanics* **210**:189–202.

Jiang ZH, Zhu ZW and Accornero F (2024a) Tensile-to-shear crack transition in the compression failure of steel-fibre reinforced concrete: Insights from AE monitoring. *Buildings* **14**:2039.

Jiang ZH, Zhu ZW, Accornero F and Wang CL (2024b) Multi-technique analysis of seawater impact on the performance of calcium sulphoaluminate cement mortar. *Construction and Building Materials* **443**:137717.

Jin L, Yu W, Du X and Yang W (2019) Mesoscopic numerical simulation of dynamic size effect on the splitting-tensile strength of concrete. *Engineering Fracture Mechanics* **209**:317–332.

Jin L, Li P, Du X and Fan L (2020) Size effect on nominal strength of circular stirrup-confined RC columns under axial compression: Mesoscale Study. *Journal of Structural Engineering* **146(3)**:04019213.

Keerthana K and Kishen JC (2020) Micromechanics of fracture and failure in concrete under monotonic and fatigue loadings. *Mechanics of Materials* **148**:103490.

Lacidogna G, Accornero F, Corrado M and Carpinteri A (2013) Crushing and fracture energies in concrete specimens monitored by Acoustic Emission. *Proceedings of the 8th international conference on fracture mechanics of concrete and concrete structures, FraMCoS*. p. 1726–1736.

Lacidogna G, Accornero F and Carpinteri A (2019) Influence of snap-back instabilities on Acoustic Emission damage monitoring. *Engineering Fracture Mechanics* **210**: 3-12.

Lacidogna G, Piana G, Accornero F and Carpinteri A (2020) Multi-technique damage monitoring of concrete beams: acoustic emission, digital image correlation, dynamic identification. *Construction and Building Materials* **242**:118114.

Li M, Hao H, Shi YC and Hao YF (2018) Specimen shape and size effects on the concrete compressive strength under static and dynamic tests. *Construction and Building Materials* **161**: 84-93.

Li WT, Jiang Z and Yu QQ (2020) Multiple damaging and self-healing properties of cement paste incorporating microcapsules. *Construction and Building Materials* **255**: 119302.

Marolt Čebašek T and Frühwirt T (2018) Investigation of creep behaviours of concrete specimens with flaws under different uniaxial loads. *Journal of Rock Mechanics and Geotechnical Engineering* **10**:151–163.

Marzec I, Tejchman J and Mroz Z (2019) Numerical analysis of size effect in RC beams scaled along height or length using elasto-plastic-damage model enhanced by non-local softening. *finite elements in analysis and design* **157**:1–20.

Morgan SP, Johnson CA and Einstein HH (2013) Cracking processes in barre granite: fracture process zones and crack coalescence. *International Journal of Fracture* **180**:177–204.

Muciaccia G, Rosati G and Luzio GD (2017) Compressive failure and size effect in plain concrete cylindrical specimens. *Construction and Building Materials* **137**:185–94.

Sinaie S (2017) Application of the discrete element method for the simulation of size effects in concrete samples. *International Journal of Solids and Structures* **108**:244–253.

Wang CL, Jiang ZH, Accornero F, Zhou SP and Ou QY (2024) Influence of seawater and salt ions on the properties of calcium sulfoaluminate cement. *Journal of Materials in Civil Engineering* **37(6)**: 04025156.

Weibull W (1951) A statistical distribution function of wide applicability. *Journal of Applied Mechanics* **18(3)**: 293–297.

Zhang H, Savija B, Xu Y and Schlangen E (2018) Size effect on splitting strength of hardened cement paste:

458 Experimental and numerical study. *Cement & Concrete Composites* **94**: 264–276.
459 Zhang P, Wang C, Gao Z and Wang F (2023) A review on fracture properties of steel fiber reinforced
460 concrete. *Journal of Building Engineering* **67**:105975.
461 Zheng Q M, Li C, He B and Jiang ZW (2022) Revealing the effect of silica fume on the flexural behavior
462 of ultra-high-performance fiber-reinforced concrete by acoustic emission technique. *Cement &*
463 *Concrete Composites* **131**:104563.
464 Zhou W, Lv ZH, Li ZY and Song X (2016) Acoustic emission response and micro-deformation behavior
465 for compressive buckling failure of multi-delaminated composites. *Journal of Strain Analysis for*
466 *Engineering Design* **51(6)**:397-407.
467 Zhu ZW, Jiang ZH, Accornero F and Carpinteri A (2024) Correlation between seismic activity and acoustic
468 emission on the basis of in-situ monitoring. *Natural Hazards and Earth System Sciences*, **24**:4133-
469 4143.